Arbitrary Waveform Generator for Quantum Information Processing with Trapped Ions

R. Bowler,[1, a)] U. Warring,[1] J. W. Britton,[1] B. C. Sawyer,[1] and J. Amini[2, b)]

[1)] *National Institute of Standards and Technology, Boulder, CO 80305, USA*

[2)] *Georgia Tech Research Institute, Atlanta, GA 30332, USA*

Atomic ions confined in multi-electrode traps have been proposed as a basis for scalable quantum information processing. This scheme involves transporting ions between spatially distinct locations by use of time-varying electric potentials combined with laser or microwave pulses for quantum logic in specific locations. We report the development of a fast multi-channel arbitrary waveform generator for applying the time-varying electric potentials used for transport and for shaping quantum logic pulses. The generator is based on a field-programmable gate array controlled ensemble of 16-bit digital-to-analog converters with an update frequency of 50 MHz and an output range of ± 10 V. The update rate of the waveform generator is much faster than relevant motional frequencies of the confined ions in our experiments, allowing diabatic control of the ion motion. Numerous pre-loaded sets of time-varying voltages can be selected with 40 ns latency conditioned on real-time signals. Here we describe the device and demonstrate some of its uses in ion-based quantum information experiments, including speed-up of ion transport and the shaping of laser and microwave pulses.

I. MOTIVATION

The building blocks for a quantum information processor involve qubits (two-level quantum systems), a universal set of operations for quantum logic, and transport of information about the processor. One realization of a quantum information processor is to use internal states of ions as qubits, where the ions are confined in a Paul trap via a combination of static and RF electric fields that forms a three-dimensional harmonic oscillator potential[1,2]. By designing a trap with multiple electrodes, arrays of trapping locations can be created between which ions can be transported. Transport is achieved via the application of time-varying electric potentials to the electrodes. Ions can then be transported between zones dedicated to particular operations such as state detection or quantum logic[3,4]. The latter is implemented by use of a sequence of laser or microwave pulses for excitations between the two levels of internal electronic states of the qubit ion.

Demonstrations of this multi-electrode trap array scheme using a suitable pair of $^2S_{1/2}$ hyperfine states of $^9Be^+$ as qubits at the National Institute of Standards and Technology (NIST) involved ion transport on a long time scale[5,6]. While each quantum logic operation typically took $\sim 10\,\mu s$, ion transport required hundreds of microseconds to remain in the adiabatic regime and thus suppressed unwanted excitations of ion oscillatory motion. A demonstration of an error correction algorithm, which is conditioned on the detection of errors, has also been carried out in this multi-electrode scheme[7]. For larger scale quantum information processing, development of larger trap architectures is necessary; some examples of the work towards larger multi-electrode trap
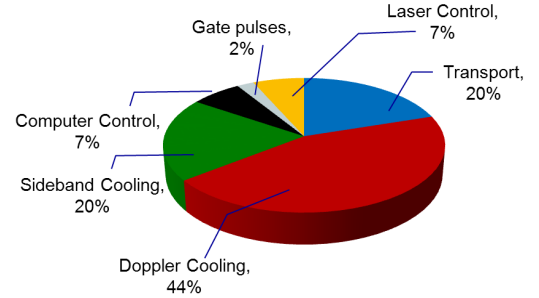
[a)] Electronic mail: ryan.bowler@nist.gov

[b)] Work was performed while this author was at the National Institute of Standards and Technology.

Figure 1. The distribution of durations between different tasks within a typical quantum logic process in Ref.[6]. The sum of quantum logic pulses amounts to a 100 μs duration, which is only 2 % of the total duration. Computer control includes preparing electronics for the experimental sequence (including the preparation of DAC output patterns for transport), laser control sets frequencies and beam powers for quantum logic, and the largest portions are due to transport and the initialization of the motional states through Doppler and Raman sideband cooling.

designs can be seen in Refs.[8–12]. However, the time scale discrepancy between quantum logic and ion transport poses a bottleneck for rapid quantum information processing. In addition, motional excitation due to electric field noise from electrode surfaces[13], the need for laser cooling to initialize motion close to the quantum ground state (via Doppler and Raman sideband cooling[2]), and the long duration of adiabatic transport poses a bottleneck if a single transport and cooling sequence exceeds a few milliseconds.

Time scales in Refs.[5,6] were primarily dominated by slow ion transport and cooling of ion motion, followed by computer control (including the preparation of electronics for transport) as another dominant temporal overhead, diagrammed in Fig. 1. Previous experiments at NIST used commercially available digital-to-analog converters (DACs) with update rates of 500 kHz for ion
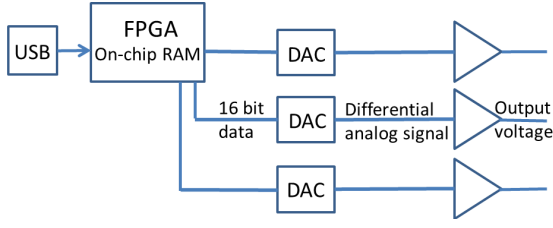
Figure 2. A flow diagram overview of the AWG. The host computer transmits waveform data via USB to the FPGA which is stored in on-chip RAM. The FPGA transmits a 16-bit digital signal derived from its RAM to each DAC, whose output is then amplified.

transport, but update rates lower than the frequencies of ion motion in the confining potential well are unsuitable for precise control of the potential on time scales similar to or faster than the ions' motional period. In addition, aliased harmonics of the 500 kHz update rate could cause significant heating of the ions' motion if not heavily filtered[10]. Large-scale error correction algorithms may require the ability to quickly alter ion transport conditioned on the detection of errors. Hence, our electronic needs for this quantum information processor scheme include fast DAC update rates compared to confinement frequencies, which can be used to reduce the duration of ion transport with low motional excitations on a quantum logic time scale, the reduction of computer control duration, the ability to control many electrodes at once, and low latency in accessing DAC output patterns (waveforms) which can be conditionally selected.

We have addressed our current technical needs by creating a fast multi-channel arbitrary waveform generator (AWG) with an update rate of 50 MHz, well beyond currently relevant trapping frequencies (typically 1 to 3 MHz). The design is easily scalable to control a large number of electrodes. We report on the design details and operation of the AWG and describe a few of its applications with trapped ions. The AWG is based on a field-programmable gate array (FPGA), which controls an ensemble of DACs that provide arbitrary analog outputs in a ±10 V range. The device is capable of simultaneously storing multiple "branches", different sets of waveforms that can be selected by use of digital logic inputs on the device with a 40 ns latency. We conclude with descriptions of experiments that demonstrate the use of AWGs in fast transport, multiple waveform branching for transport, and pulse shaping applications for ion-based quantum information processing.

II. DESIGN

A. Hardware

The AWG uses the Xilinx Spartan-3E XC3S500E PQ208[14] model FPGA to control three 16-bit Analog

Devices AD9726[14] DACs. The FPGA logic was coded in VHDL using the Xilinx ISE Design Suite[14]. The AD9726 DAC was chosen because of its high speed, its linearity, and its use of low voltage differential signal (LVDS) which is resistant to pick-up noise. A host computer provides waveform specifications that are stored in three segments of independent static random access memory (RAM) in the FPGA for each connected DAC channel (provided by a total of 360 kilobits of on-chip RAM). The FTDI FT245RL USB-to-parallel-FIFO[14] provides an interface to connect a host computer to the FPGA memory, across which waveform data is uploaded to RAM. An overview for the operation of the AWG is shown in Fig. 2.

The AWG has a USB connection to the host computer and a 50 MHz crystal oscillator to provide a clock signal. There are two types of AWGs, a "master" and a "slave", with a small number of hardware differences. Slaves are connected to the master through board-to-board interconnects, through which the waveform data and the clock signal are routed to be processed by their respective FPGAs. One master and two slaves can be connected to provide up to nine synchronous channels on a single USB connection. Separate masters are referenced to different oscillators and hence have timing offsets of at most 20 ns, though this is so far negligible in our experiments. Each AWG master is identified over the USB connection by a unique serial number programmed into the FT245RL, so in principle any number of channels can be controlled from a single computer (limited by the computer's USB architecture).

Groups of each channel's RAM can be configured into eight independent waveform branches of user-defined sizes externally selected with three TTL user inputs. The TTL inputs switch waveforms with 40 ns (two clock cycles) latency and allow the user to switch between waveforms in real-time with the rest of the experiment in response to events. There is an additional input TTL trigger on each master for signaling the start of a waveform on all connected channels; the rising edge triggers the start of reading waveform data from the selected branch on all channels. By tying more than one master to a single TTL, many masters (and their respective slaves) can be run synchronously. Each waveform branch may further be broken up into a sequence of waveform "steps", such that in a single branch a set of TTL triggers will run a sequence of waveforms.

The DACs are clocked from a 50 MHz signal generated by the FPGA. Each DAC's output is referenced to a precision 1.25 V source (Linear Technology LTC6652[14]), specified to have 10 ppm/°C and 2.1 ppm noise, for stable and consistent potentials out of every channel. The differential signal outputs of each DAC are then sent to high-speed amplifiers (Analog Devices AD8250[14]) to provide the final output potentials; the DAC and amplifier system is configured for a ±10 V output with 16-bit linear resolution, stable down to roughly 30 μV and with $\sim 1\,\Omega$ output impedance. A 50 Ω resistor can be added in series with the output to prevent ringing in long ca-
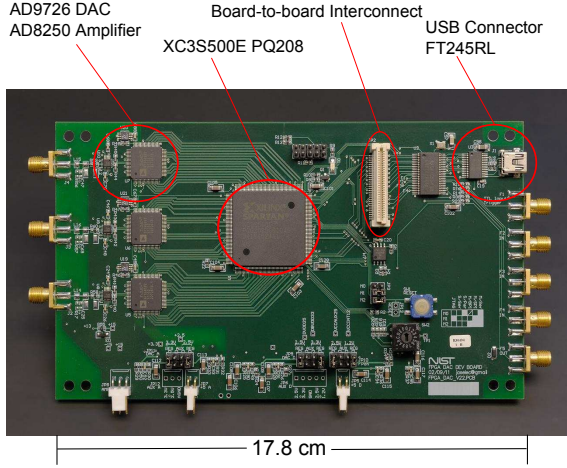
Figure 3. A master board. The key components described in the text are highlighted. The host computer communicates with the master board via USB. The FT245RL handles the interface with the XC3S500E PQ208 FPGA on up to three boards (a master and two slaves) on a shared communication channel through a board-to-board interconnect. The FPGA drives three AD9726 DACs whose output is fed to AD8250 amplifiers, which creates the final three output potentials.

bles. After the resistor we observe a white noise power spectral density of ~120 nV/$\sqrt{\text{Hz}}$ with an external 50 Ω load. The amplifier's output has a measured slew rate of 40 V/μs; although this limits the voltage swing at each clock update, it is sufficient for our experimental implementations. A photograph of a master board is shown in Fig. 3 with the discussed components highlighted.

B. Software

The host computer can specify the waveforms in one of four modes as follows: (1) Output specified by a potential during each 20 ns clock cycle update, (2) Output given by potentials for specified durations, (3) Output given in terms of quadratic polynomials specified by a duration and coefficients, and (4) Output specified in terms of cubic polynomials (of primary interest, cubic spline interpolation for 1st and 2nd derivative continuity in the waveform). Options 2, 3, and 4 can provide increasing levels of data compression. This is often necessary to overcome limited amounts of RAM and reduce waveform upload durations from the host computer. When operating in the 4th mode, up to 614 polynomials can be stored in each channel's RAM. The interval between a TTL trigger and when a waveform begins to run depends on the time required to read the initial data from memory (longest is the 4th mode where 240 ns, or twelve clock cycles, are required before the waveform begins), but after this initial delay the memory is read continuously while the waveform runs so there is no slow-down in run time.
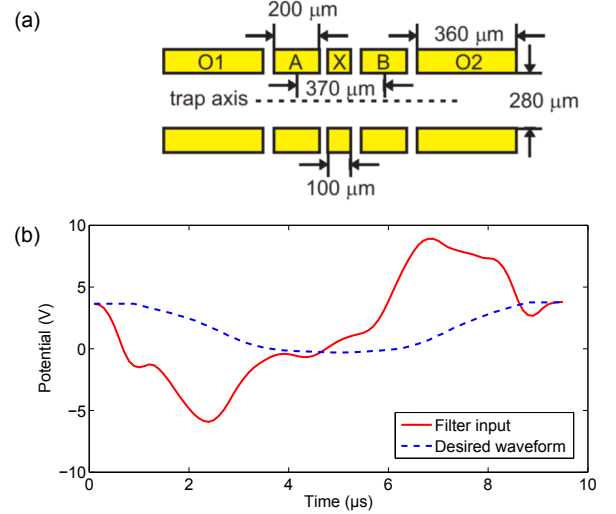
Our in-house data acquisition system provides con-

Figure 4. (a) Schematic of the ion trap electrode structure showing the two diagonally opposite segmented DC electrodes (not to scale). Outer electrodes O1 and O2 are used to fine tune the potential while ions move over electrodes A, X, and B during the experiments in Ref.[16]. (b) Example filter compensation for electrode X during transport of an ion from over electrode A to over electrode B. The desired waveform is generated from simulation and the potentials generated by the AWG must account for filter distortion. The waveform from the AWG must overshoot in time and voltage to achieve the desired 8 μs transport potentials.

trol of parameters in our experiments: the timing and sequences of most quantum logic pulses via a separate FPGA timing system, the waveform upload to the AWGs (including specifications for the channel and branch configuration for each waveform), and any other dynamic experimental parameters (see Ref.[15] for details). This system controls experimental TTL signals including the run trigger and branch switching logic for the AWG, along with switching and timing TTL signals for various quantum logic pulses. The FT245RL has a support library of C++ commands provided by the manufacturer, which is used in the data acquisition system for communication between the host computer and the AWGs.

III. EXPERIMENTAL APPLICATIONS

A. Fast Ion Transport

For rapid quantum information processing in a multi-electrode trap architecture, ion transport should occur on a time scale comparable to quantum logic (e.g. $\sim 10\,\mu$s for ion based systems) or faster. The high speed of the AWG relative to confinement frequencies in a linear Paul trap enables variation of electrode potentials for ion transport within a fraction of the ion oscillation period. We employed the AWG for fast, diabatic transport of ions[16], where the transport waveforms accelerated

and decelerated the ions within the ion oscillation period and observed a low final motional excitation in a single transport. In our experiments, the AWG produced the time-varying electric potentials in a multi-electrode linear Paul trap (diagrammed in Fig. 4a) to transport one and two ^{9}Be$^+$ ions in 8 μs across 370 μm at a constant velocity, with the ions confined in a $\omega_z/2\pi \sim 2$ MHz potential well. We also separated two ^{9}Be$^+$ originally held in a single confining well in 55 μs into two separate trap zones. These experiments demonstrated that transport and separation over relevant distances on quantum logic time scales can be performed with suppressed excitation in the trapped ions' final motional state.

A complication in our experiments arises from a chain of resistor-capacitor (RC) low-pass filters that is applied to each electrode to reduce electric field noise from external sources. Due to the high speed of the fast ion transport waveforms, we must pre-compensate for the low-pass effects of the filters in order to achieve the desired time-dependence of the electrode potentials[17]. The filters for each electrode, from AWG-side to trap-side, are a pair of 200 kHz low-pass RC filters followed by one 800 kHz low-pass RC filter (see Fig. 5). The input potential V_{input} to a single stage of the RC filters in the filter chain are related to the desired output potential V_{output} by

$$V_{input} = V_{output} + R_i C_i \frac{dV_{output}}{dt}$$
$$+ (V_{output} - V_{prev})\frac{R_i}{R_{prev}}, \quad (1)$$

where R_i and C_i are the RC component values of the ith layer of the filter chain and V_{prev} and R_{prev} are from the solution to the previous layer of filtering trap-side. One result of numerically solving for the effects of the filter system is exemplified in Fig. 4b. The transport waveforms, including that shown in Fig. 4b, were specified by cubic splines that occupied ~ 6 % of each channel's memory.

Despite the filters' time constants on the scale of a few microseconds, we can still run a waveform to faithfully transport ions in our trap in 8 μs. A convenient characterization of the oscillatory motion is the average occupation of motional quanta $\bar{n}$. In Refs.[5,6], motion was initalized to $\bar{n} \sim 0.1$ after cooling. However, ion transport (in this case, separation) was typically on the time scale of 1 ms, and after separating ions into separate trap zones, typical oscillatory motion was excited to $\bar{n} \sim 5$ which required re-cooling. Re-cooling, with respect to Fig. 1, consisted of approximately three milliseconds of Doppler and Raman sideband cooling. Using the AWG in the experiments in Ref.[16], we achieved $\bar{n} \approx 0.2$ after single ion transport in 8 μs and $\bar{n} \approx 2$ after separating two ions into separate trap zones in 55 μs. This is not only on a much shorter time scale but also requires less re-cooling, to be implemented in future quantum information processing experiments to be able to compare
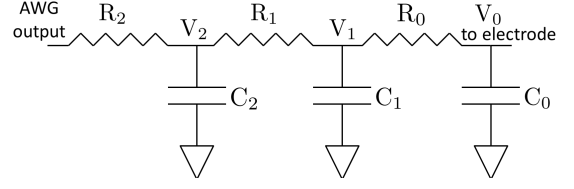

Figure 5. A diagram of our low-pass RC filter system connected to each electrode. The indices of each passive component correspond to the filter layer, and the voltages correspond to those governed by Eq. 1 with V_0 the final stage applied to the electrode. The values are $\{R_2, R_1, R_0\} = \{820, 820, 240\}$ Ω and $\{C_2, C_1, C_0\} = \{1, 1, 0.82\}$ nF.

directly to Fig. 1. Different diabatic transport methods using a waveform generator with a 2.5 MHz update rate were demonstrated with ions confined in a 1.4 MHz potential well[18] with similar low-excitation results for transport. However, this update rate is too slow for the level of control over the accelerations and velocities that we desire.

B. Waveform branching

The capability to quickly switch between waveform branches allows complex sequences of waveforms to be built up from a series of simpler component waveforms. For example, the experiments in Ref.[6] required two ^{9}Be$^+$ qubit ions to be in a shared trap zone for two-qubit operations, separated to distinct zones for one-qubit operations, and recombined; the full sequence required as many as 16 separation and recombination waveforms in a single process. We used three waveform branches pre-loaded into AWG memory and selected with TTL inputs during the experiments: (1) the static trap potential, (2) the separation waveform, and (3) the recombination waveform. The experimental sequences of these three waveform branches were concatenated on the fly without the necessity to upload a new set of waveforms for each sequence, enabled by the AWG branching capability.

C. Shaped Microwave Pulses

Another application of the AWG involves the shaping of laser and microwave pulses for quantum logic. We demonstrate the pulse shaping of a microwave signal at ~ 1.7 GHz that drives a hyperfine transition in ^{25}Mg$^+$. For the experiments in Ref.[19], we used the pulse shaping to prevent "ringing" of high power (~ 45 dBm) pulsed microwave signals during turn on/off. To circumvent this ringing, we ramped up the power of the signals over 10 μs. Using an analog multiplier, one channel from the AWG was used to amplitude modulate the microwave signal. The waveforms from the AWG can be varied in duration and amplitude. After this pulse shaping, the signal
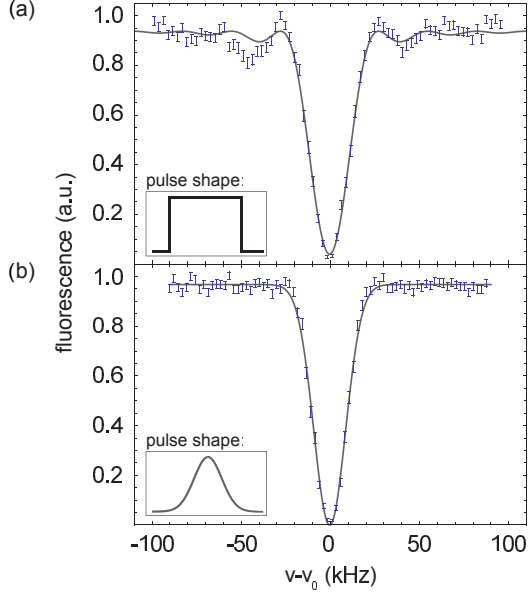
Figure 6. Temporal pulse shaping of a microwave signal using the AWG to specify the profile. The microwave drives the hyperfine transition in ^{25}Mg$^+$. Shown is the ion fluorescence vs. microwave frequency. Here $\nu_0 = 1.7$ GHz denotes the frequency splitting of the two hyperfine levels. (a) We used a rectangular pulse shape, duration 20 μs, and found the corresponding sinc^2 form in frequency space. (b) We used a Gaussian pulse shape and found the corresponding Gaussian form in frequency space. The FWHM pulse duration is 45 μs, with the Gaussian tail truncated to a total duration of four times the FWHM.

is amplified and used to drive the hyperfine transition. In Fig. 6, we show resonances (in frequency space) of the hyperfine transition followed by a state-dependent fluorescence measurement for two cases (here done with ~ 5 dBm to minimize the impact of ringing): a rectangular pulse shape (Fig. 6a), and a Gaussian pulse shape (Fig. 6b). We find that the transition profiles correspond to the Fourier transform of the pulse shape, a sinc^2 and a Gaussian, respectively, with pulse durations chosen for approximately equal full width at half max (FWHM) for each profile.

D. Shaped Optical Pulses

Laser beams are commonly used for motional state preparation and generation of spin-spin entanglement in ion-based quantum information processing. As the ion-laser interactions are not typically continuous, a computer-controlled light modulator is used to pulse on and off the laser beams. Acousto-optic modulators (AOM) can be used as optical switches; actuation is achieved by a TTL-controlled RF switch. The resulting optical pulse has a rise-time of $\sim 1\,\mu$s, set by the acoustic wave transit time over the laser beam in the AOM. For some applications, greater control over the optical pulse amplitude is desired.

A RF mixer is a passive circuit that can be used for high-bandwidth amplitude modulation of a RF carrier. The amplitude of the modulation current $i_{\rm IF}$ applied to the mixer's IF port varies the RF-port to local oscillator (LO)-port coupling. As the coupling is inherently nonlinear with $i_{\rm IF}$, it is convenient to use closed-loop feedback to obtain a linear response. In this case the feedback is from a light-sensing photodiode (PD). A collateral benefit of using a closed loop to linearize the response is that amplitude noise in the laser beam is attenuated over the loop bandwidth.

The current $i_{\rm IF}$ sent to the mixer's IF port is determined by an analog proportional-integral (PI) servo with an integrator track-and-hold (TAH) capability (a schematic of the experimental set up is shown in Fig. 7). The PI is configured to minimize $|V_+ - V_-|$, where V_+ is the PD voltage and V_- is an output channel of the AWG. The TAH prevents undesired activity from the integrator when the laser is "off", e.g. due to non-zero photocurrent from the PD. Clamping $i_{\rm IF} > 0$ prevents bistability of the loop. Laser beam attenuation is controlled by utilizing the -1 diffracted order of the AOM for the laser (often in a double-pass configuration). To attenuate the laser beam intensity beyond that permitted by minimum LO-RF transmission, we employ an RF switch to extinguish the -1 diffracted order of the AOM.

A near-resonant laser beam is used to laser cool the harmonic motion of ^{9}Be$^+$ ions ($\omega_z/2\pi \sim 1$ MHz) with a 10 % duty cycle in a Penning Trap with ~ 200 ions[20]. During Doppler laser cooling, the ion plane is slightly displaced from the trap center by the cooling light propagating perpendicular to the plane. When this cooling laser is switched off quickly relative to ω_z (non-adiabatic), the ion plane oscillates in the trap with a coherent amplitude corresponding to $\bar{n}$ which is consistent with a thermal energy of 5-10 mK, well above the Doppler cooling limit of 0.4 mK. To achieve the Doppler limit for center-of-mass motion, we ramp the cooling laser intensity adiabatically over $\sim 100\,\mu$s using a $\sin(\omega t)^2$ temporal profile, where $\omega/2\pi \sim 2.5$ kHz is the ramp rate.

IV. SUMMARY

We have designed and constructed an AWG with voltage outputs with a range of ± 10 V and with a 50 MHz update rate. The FPGA provides versatile control over and storage of waveforms. The output can be used to control trapping potentials in ion-based experiments, and several AWG units can be combined to control many trap electrodes. The AWG can also be used for temporal shaping of laser and microwave pulses. Branching capabilities controlled by TTL logic allow quick switching between waveforms with 40 ns latency that can be conditioned on experimental parameters, a feature useful for error correction algorithms. We gave some examples of more
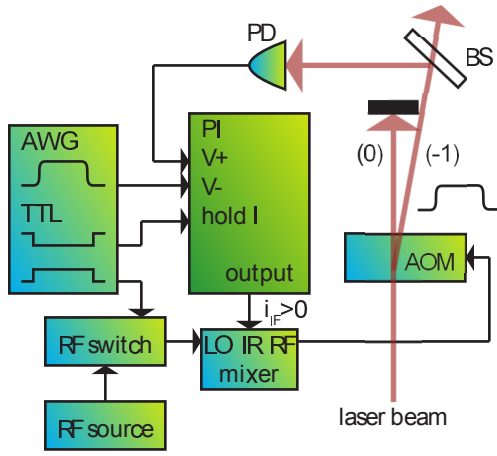
Figure 7. Laser beam amplitude modulation circuit using a single DAC channel of the the AWG, a mixer, and a PI controller in a feedback loop.

detailed accounts of the AWG's capabilities in the applications of high-speed transport of ions and the shaping of quantum logic pulses.

REFERENCES

[1] J. I. Cirac and P. Zoller, Phys. Rev. Lett. **74**, 4091 (1995).
[2] D. J. Wineland, C. Monroe, W. M. Itano, D. Leibfried, B. E. King, and D. M. Meekhof, J. Res. Natl. Inst. Stand. Technol. **103**, 259 (1998).
[3] J. I. Cirac and P. Zoller, Nature **404**, 579 (2000).
[4] D. Kielpinski, C. Monroe, and D. Wineland, Nature **417**, 709 (2002).
[5] D. Hanneke, J. P. Home, J. D. Jost, J. M. Amini, D. Leibfried, and D. J. Wineland, Nature Physics **6**, 13 (2010).
[6] J. P. Gaebler, A. M. Meier, T. R. Tan, R. Bowler, Y. Lin, D. Hanneke, J. D. Jost, J. P. Home, E. Knill, D. Leibfried, and D. J. Wineland, Phys. Rev. Lett. **108**, 260503 (2012).
[7] J. Chiaverini, D. Leibfried, T. Schaetz, M. D. Barrett, R. B. Blakestad, J. Britton, W. M. Itano, J. D. Jost, E. Knill, C. Langer, R. Ozeri, and D. Wineland, Nature **432**, 602 (2004).
[8] G. Huber, T. Deuschle, W. Schnitzler, R. Reichle, K. Singer, and F. Schmidt-Kaler, New J. Phys. **10**, 013004 (2008).
[9] J. M. Amini, H. Uys, J. H. Wesenberg, S. Seidelin, J. Britton, J. J. Bollinger, D. Leibfried, C. Ospelkaus, A. P. VanDevender, and D. J. Wineland, New J. Phys. **12**, 033031 (2010).
[10] R. B. Blakestad, C. Ospelkaus, A. P. VanDevender, J. H. Wesenberg, M. J. Biercuk, D. Leibfried, and D. J. Wineland, Phys. Rev. A **84**, 032314 (2011).
[11] D. T. C. Allcock, T. P. Harty, H. A. Janacek, N. M. Linke, C. J. Ballance, A. M. Steane, D. M. Lucas, R. L. Jarecki Jr., S. D. Habermehl, M. G. Blain, D. Stick, and D. L. Moehring, Applied Physics B **107**, 913 (2012).
[12] S. C. Doret, J. M. Amini, K. Wright, C. Volin, T. Killian, A. Ozakin, D. Denison, H. Hayden, C.-S. Pai, R. E. Slusher, and A. W. Harter, New J. Phys. **14**, 073012 (2012).
[13] Q. A. Turchette, D. Kielpinski, B. E. King, D. Leibfried, D. M. Meekhof, C. J. Myatt, M. A. Rowe, C. A. Sackett, C. S. Wood, W. M. Itano, C. Monroe, and D. J. Wineland, Phys. Rev. A **61**, 063418 (2000).
[14] Commercially sourced materials and services are identified in this paper in order to specify the designs adequately. Such identification is not intended to imply recommendation or endorsement by NIST, nor is it intended to imply that the materials or equipment identified are necessarily the best available for the purpose.
[15] C. Langer, *High fidelity quantum information processing with trapped ions*, Ph.D. thesis, Department of Physics, University of Colorado, Boulder (2006).
[16] R. Bowler, J. Gaebler, Y. Lin, T. R. Tan, D. Hanneke, J. D. Jost, J. P. Home, D. Leibfried, and D. J. Wineland, Phys. Rev. Lett. **109**, 080502 (2012).
[17] J. P. Home, private communication.
[18] A. Walther, F. Ziesel, T. Ruster, S. T. Dawkins, K. Ott, M. Hettrich, K. Singer, F. Schmidt-Kaler, and U. Poschinger, Phys. Rev. Lett. **109**, 080501 (2012).
[19] C. Ospelkaus, U. Warring, Y. Colombe, K. R. Brown, J. M. Amini, D. Leibfried, and D. J. Wineland, Nature **476**, 181 (2011).
[20] B. C. Sawyer, J. W. Britton, A. C. Keith, C.-C. J. Wang, J. K. Freericks, H. Uys, M. J. Biercuk, and J. J. Bollinger, Phys. Rev. Lett. **108**, 213003 (2012).